



**UNIVERSITY OF LEEDS**

This is a repository copy of *Closed-form control oriented model of highly flexible manipulators*.

White Rose Research Online URL for this paper:

<https://eprints.whiterose.ac.uk/143463/>

Version: Accepted Version

---

**Article:**

Scaglioni, B [orcid.org/0000-0003-4891-8411](https://orcid.org/0000-0003-4891-8411), Bascetta, L, Baur, M et al. (1 more author) (2017) Closed-form control oriented model of highly flexible manipulators. *Applied Mathematical Modelling*, 52. pp. 174-185. ISSN 0307-904X

<https://doi.org/10.1016/j.apm.2017.07.034>

---

(c) 2017, Elsevier Inc. This manuscript version is made available under the CC BY-NC-ND 4.0 license <https://creativecommons.org/licenses/by-nc-nd/4.0/>

**Reuse**

This article is distributed under the terms of the Creative Commons Attribution-NonCommercial-NoDerivs (CC BY-NC-ND) licence. This licence only allows you to download this work and share it with others as long as you credit the authors, but you can't change the article in any way or use it commercially. More information and the full terms of the licence here: <https://creativecommons.org/licenses/>

**Takedown**

If you consider content in White Rose Research Online to be in breach of UK law, please notify us by emailing [eprints@whiterose.ac.uk](mailto:eprints@whiterose.ac.uk) including the URL of the record and the reason for the withdrawal request.



[eprints@whiterose.ac.uk](mailto:eprints@whiterose.ac.uk)  
<https://eprints.whiterose.ac.uk/>

# Closed-Form Control Oriented Model of Highly Flexible Manipulators

Bruno Scaglioni<sup>\*a,b</sup>, Luca Bascetta<sup>a</sup>, Marco Baur<sup>a</sup>, Gianni Ferretti<sup>a</sup>

<sup>a</sup>*Politecnico di Milano, Dipartimento di Elettronica, Informazione e Bioingegneria,  
20133 Milan, Piazza Leonardo da Vinci 32, Italy (e-mail:*

*{bruno.scaglioni,luca.bascetta,gianni.fettetti,marco.baur}@polimi.it).*

<sup>b</sup>*MUSP Lab, Via Tirrotti 9, Le Mose, 29122 Piacenza, Italy (e-mail:  
bruno.scaglioni@musp.it).*

---

## Abstract

This paper first presents a highly flexible 3D manipulator with links of arbitrary shape, then develops a closed-form dynamic model that best describes it. The model is based on a Newton-Euler formulation and the substructuring method is used to account for large deformations. The formulation of the motion equations starts from a data set which can be either analytically or numerically computed by finite elements(FE) codes. Simulation has been used to validate the model and compare the results with those of two different multibody software and one experimental, which was obtained from the Multi-Elastic-Link Robot Identification Dataset (MERIt), developed by the TU Dortmund. Then, thanks to the approach here adopted, an integral manifold model is derived, suitable for advanced control system design.

*Keywords:* Flexible manipulators, Newton Euler model, closed form model, manipulator control, dynamics, flexible multibody

---

## 1. Introduction

There are many papers in the literature on the modelling and control of flexible manipulators of robots (e.g., ). Space exploration, for example, requires the design of lightweight robots that are capable of moving heavy items, but yet flexible. The design of such robots, mainly their manipulators, are of interest to this paper. [1], [2], [3]. Nowadays, the interest for modelling flexible structures is even spreading to industrial robotics [4], where the increase of performance requirements demands for a continuous increase in

control loop bandwidths, that forces the introduction of flexible arm models instead of the more traditional rigid ones [5].

For many years, however, the development of model-based estimation and control strategies was limited to very simple structures [6], and manipulators were modelled as chains of simplified slender and rectangular cross-section beams. Indeed, the derivation of a dynamic model of a flexible manipulator characterised by links with a generic shape, that is suitable for real-time estimation and control, is a complex task, where feasibility and pertinence of the solution are often limited by the complexity of the flexible dynamics, which often introduce a heavy computational burden, or, in the worst case, can be tackled only by means of multibody tools, which however are not suitable for model-based control design.

The main problem with structural flexibility modelling, namely the approximation of the infinite dimensional model with a finite dimensional one, is commonly solved by means of two techniques: the assumed mode method (AMM) [7, 8], where the deformation field is defined over the entire link, and the finite element method (FEM) [9], where the deformation field is described over subdomains. Both AMM and FEM methods are usually adopted in conjunction with the floating frame of reference (FFR) approach [10], where the superposition of large body motion and small linear deformations is expressed in a local reference frame, attached to each flexible body. FFR uses a linear combination of space-dependent shaped functions with time-dependent weights of elastic coordinates to represent each deflection point. One of the great advantages of the FFR approach is the possibility, provided by commercial FE codes, to obtain the shape functions for arbitrary shapes. Most commercial codes [11, 12] can reduce models from a huge number of nodal coordinates to a small amount of modal coordinates by generating modal shape functions, allowing to recovery the spatial displacement of connectors as a combination of modal coordinates. This can be achieved by means of the component mode synthesis (CMS) method [13], based on the Craig-Bampton approach [14], as currently carried on by all commercial codes, or through recently proposed methods, like Krylov subspaces [15], proper orthogonal decomposition [16] or other non-modal order reduction techniques [17].

The standard FFR approach is however not feasible in the context of large deflections, since the hypothesis of small linear deformations superimposed to a large rigid body motion no longer holds. In order to overcome the restrictions imposed by the FFR method, the Absolute Nodal Coordinate Formulation (ANCF) [18] has been developed. In fact, in the ANCF ap-

proach, beams and shells are considered as isoparametric elements, hence no infinitesimal or finite rotations are used, and, consequently, these elements can account for arbitrary large deformation problems. In this formulation the position vector of an arbitrary point on the flexible body is defined in terms of a global shape function and a vector of nodal coordinates. On the other hand, the ANCF has been mainly applied to beams and shell elements, and it is not directly applicable to complex geometries and to automatic analysis by means of FE packages.

Accuracy of results for large deformation fields can be anyway achieved, in the context of the FFR approach, by means of the substructuring technique [19]. Highly flexible bodies can thus be substructured into several elements, while applying to each element the theory of linear elasticity. This approach, adopted also in this work, is particularly feasible for long and thin structures like robotic manipulators, helicopter blades and wind turbines.

This paper starts by introducing a dynamic model that represent 3D flexible manipulators. The formulation of the manipulators' motion equations and the spatial vector notation are from the Newton-Euler method [20]. The model is formulated in closed form with respect to joint and elastic coordinates, applying the substructuring approach in order to cope with highly flexible structures. Links of arbitrary shape are considered, whose relevant data can be acquired as the output of most commercial FEM packages [21]. The model is then expressed in terms of the integral manifold approach [22], where two separate dynamic systems are identified, representing the on-manifold and the off-manifold dynamics, respectively. It must be pointed out that the proposed formulation is suitable for manipulators made by open kinematic chains of flexible links and rotational joints, hence, parallel manipulators and robots with prismatic joints are beyond the scope of this work. The approach proposed in this paper is based on a result, exhaustively illustrated in [25] where the closed form model is defined. The improvements here described consist in a further theoretical result regarding the the manipulators characterized by highly flexible links and the related model validation. Moreover, the closed form model is used as starting point for the development of a control-oriented model whose formulation is completely new with respect to literature. The proposed model is finally validated by means of comparison with different mathematical formulations. The proposed formulation allows to consider manipulators with links of general shape and provides two different modelling tools, allowing the model to be used during the analysis and design tasks, or in the synthesis of model based estimation

and control algorithms [23]. The paper is organized as follows. Section 2 describes how to correctly setup the preprocessing stage in order to retrieve link's data, in Section 3 the closed-form model of the 3D flexible manipulator is derived and the substructuring technique, developed in order to account for high flexibility, is presented. Section 4 introduces two case studies used to validate the closed-form model, while in Section 5 the derivation of the control oriented model of a flexible body and its validation are described. Section 6 concludes the paper.

## 2. Generating the Flexible Body Data Set

As previously mentioned, the design of model-based control and estimation algorithms was seriously hampered by the complexity of the derivation of lumped parameter models describing the distributed flexibility of bodies. In fact, this procedure can be performed analytically only in the case of very simple geometries and adopting some simplifying assumptions, as in the case of the Euler beam [24].

In this respect, the introduction of a FEM preprocessing stage allows to consider more complex geometries, e.g. manipulators' arms with articulated shapes (see Figure 1), while not resulting, however, in a closed-form model suitable for real-time implementations.

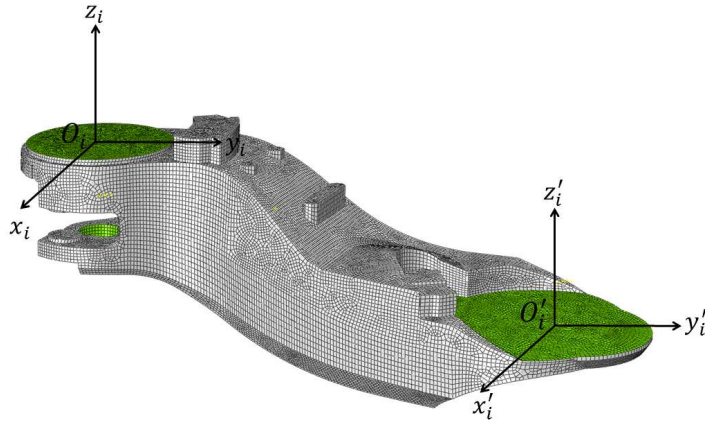


Figure 1: FEM preprocessing

On the other hand, most commercial FEM packages can directly provide the flexible body data, required for the derivation of such a closed-form

model, as the output of a substructuring procedure based on the CMS method [14], that is constituted by the following steps:

- *Selection of connectors.* Points corresponding to a reference frame must be identified as boundary points of the substructuring analysis (Fig. 1).
- *Meshing.* The CAD model must be meshed, with a node corresponding to every reference point identified in the previous stage.
- *Coupling.* Every contact region of the body, highlighted in green in Figure 1, must be kinematically coupled to a corresponding reference point through the MPC (Multi Point Constraint) construct in the FE model.
- *Boundary conditions.* The node corresponding to the origin of the FFR must be clamped.
- *Choice of retained eigenmodes.* There is no formal procedure for the choice of the eigenmodes, but it is suggested to consider at least two or three modes for every direction of interest, unless special requirements in terms of frequency content must be considered.
- *Substructuring.* The substructuring analysis<sup>1</sup> is usually performed automatically by most commercial FE solvers and the results are stored in a modal neutral file (`.mnf`)<sup>2</sup>.

The body data obtained as the output of the procedure are listed in Table 1, where the inertia invariants account for the body mass distribution, and the shape function matrices are used as a basis to describe the deformation field (see next Section for further details).

---

<sup>1</sup>The substructuring analysis performed by FEM packages must not be confused with the substructuring of flexible bodies described at the end of Section 3 to account for large deformations.

<sup>2</sup>A dedicated parsing tool [21] has been developed in order to store all the relevant data included in the `.mnf` file in a format (HDF5 file) that can be used in Modelica and MATLAB environments.

Table 1: Body data

$M_i$	Number of modal coordinates
$I_i^1, I_i^2, I_{j,i}^3, I_i^4, I_{j,i}^5, I_i^6, I_i^7, I_{j,i}^8, I_{jk,i}^9$	Inertia invariants
$\mathbf{K}_{e,i}$	Structural stiffness matrix
$\mathbf{S}_i, \hat{\mathbf{S}}_i$	Shape function matrices
$\bar{\mathbf{u}}_{0i}$	Undeformed relative position between FFRs

### 3. Closed-Form Manipulator Model

The results of the FEM analysis (Table 1) can be now used to write the closed-form motion equations of a flexible manipulator:

$$\mathcal{M}_{\theta\theta}(\boldsymbol{\theta}, \mathbf{q})\ddot{\boldsymbol{\theta}} + \mathcal{M}_{\theta q}(\boldsymbol{\theta}, \mathbf{q})\ddot{\mathbf{q}} + \mathcal{C}_\theta(\boldsymbol{\theta}, \mathbf{q}, \dot{\boldsymbol{\theta}}, \dot{\mathbf{q}}) = \boldsymbol{\tau} , \quad (1)$$

$$\mathcal{M}_{\theta q}^T(\boldsymbol{\theta}, \mathbf{q})\ddot{\boldsymbol{\theta}} + \mathcal{M}_{qq}(\boldsymbol{\theta}, \mathbf{q})\ddot{\mathbf{q}} + \mathcal{D}_e\dot{\mathbf{q}} + \mathcal{K}_e\mathbf{q} + \mathcal{C}_q(\boldsymbol{\theta}, \mathbf{q}, \dot{\boldsymbol{\theta}}, \dot{\mathbf{q}}) = \mathbf{0} , \quad (2)$$

where  $\boldsymbol{\theta} = \text{col}\{\theta_i\} \in \mathbb{R}^N$  and  $\theta_i$  are the angles of the joints,  $\mathbf{q} = \text{col}\{\mathbf{q}_i\} \in \mathbb{R}^M$ , where  $\mathbf{q}_i$  is the vector of modal coordinates of link  $i$ ,  $\boldsymbol{\tau} = \text{col}\{\tau_i\} \in \mathbb{R}^N$  where  $\tau_i$  are and the joint torques. Consequently, the total number of modal coordinates is  $M = \sum_{i=1}^N M_i$ . The derivation of model (1,2) is here briefly sketched, further details can be found in [25].

The local Floating frame of reference, relative to link  $i$  is defined as  $\{O_i, \mathbf{x}_i, \mathbf{y}_i, \mathbf{z}_i\}$  (Fig. 2). Another local frame  $\{O'_i, \mathbf{x}'_i, \mathbf{y}'_i, \mathbf{z}'_i\}$  is defined having the same undeformed orientation of the FFR of link  $i$ , and coinciding origin with the FFR of link  $i + 1$ .

Let  $\theta_i$  be the angle of the joint connecting link  $i$  to link  $i - 1$ , and let  $\hat{\mathbf{z}}'_{i-1}$  be the rotation axis of the revolute joint connecting link  $i$  to link  $i - 1$  in the frame  $\{O'_{i-1}, \mathbf{x}'_{i-1}, \mathbf{y}'_{i-1}, \mathbf{z}'_{i-1}\}$ . For the sake of simplicity, only revolute joints are considered. In the particular case of flexible manipulators with prismatic joint, the relative displacement between the FFR of link  $i$  and link  $i + 1$  depends on the  $i+1^{\text{th}}$  joint coordinate. Consequently, the point of application of the forces exchanged between the links varies with the relative positions of the links, but the shape functions derived from the finite element analysis are referred to a single point, hence an interpolation procedure should be developed.

Accordingly, the rotation matrix  $\mathbf{A}_{i+1}$  of the  $(i + 1)$ -th frame with respect to the world frame and the position  $\mathbf{p}_{i+1}$  of the origin  $O_{i+1}$  of the  $(i + 1)$ -th

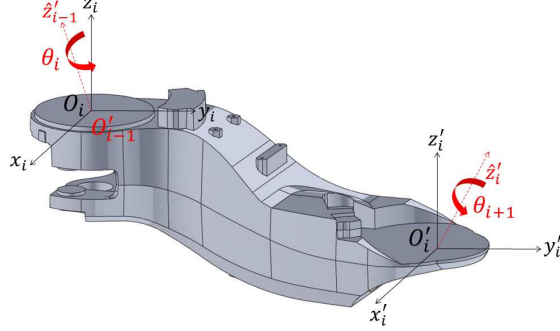


Figure 2: Reference frames

frame in the world reference frame, are given by<sup>3</sup>

$$\mathbf{A}_{i+1} = \mathbf{A}_i \left[ \mathbf{U} + \left( \widetilde{\hat{\mathbf{S}}_i \mathbf{q}_i} \right) \right] \bar{\mathbf{A}}_i(\hat{\mathbf{z}}'_i, \theta_{i+1}) , \quad (3)$$

$$\mathbf{p}_{i+1} = \mathbf{p}_i + \mathbf{A}_i \bar{\mathbf{u}}_{0,i} + \mathbf{A}_i \mathbf{S}_i \mathbf{q}_i , \quad (4)$$

where  $\mathbf{A}_i$  is the  $(3 \times 3)$  rotation matrix relating the local FFR and the world reference frame, the  $[3 \times M_i]$  shape function matrices  $\mathbf{S}_i$ ,  $\hat{\mathbf{S}}_i$  define *small* displacements and rotations of the frame  $\{O'_i, \mathbf{x}'_i, \mathbf{y}'_i, \mathbf{z}'_i\}$  with respect to the FFR, matrix  $\bar{\mathbf{A}}_i$  defines a rotation of the frame  $\{O_i, \mathbf{x}_{i+1}, \mathbf{y}_{i+1}, \mathbf{z}_{i+1}\}$  of an angle  $\theta_{i+1}$  about an axis defined in the frame  $\{O'_i, \mathbf{x}'_i, \mathbf{y}'_i, \mathbf{z}'_i\}$  by the constant unit vector  $\hat{\mathbf{z}}'_i$ .

Differentiating eqs. (3,4) twice with respect to time, the linear and angular accelerations of the  $(i+1)$ -th frame can be obtained<sup>4</sup>:

$$\dot{\mathbf{v}}_{i+1} = \dot{\mathbf{v}}_i - \tilde{\mathbf{p}}_{i+1,i} \dot{\boldsymbol{\omega}}_i + \mathbf{A}_i \mathbf{S}_i \ddot{\mathbf{q}}_i + \dot{\mathbf{v}}'_{i+1} , \quad (5)$$

$$\dot{\boldsymbol{\omega}}_{i+1} = \dot{\boldsymbol{\omega}}_i + \mathbf{A}_i \hat{\mathbf{A}}_i \hat{\mathbf{z}}'_i \ddot{\theta}_{i+1} + \mathbf{A}_i \hat{\mathbf{S}}_i \ddot{\mathbf{q}}_i + \dot{\boldsymbol{\omega}}'_{i+1} , \quad (6)$$

where  $\dot{\mathbf{v}}'_{i+1}$  and  $\dot{\boldsymbol{\omega}}'_{i+1}$  depend on the angular velocity  $\boldsymbol{\omega}_i$ . In turn, adopting

<sup>3</sup>Given a vector  $\mathbf{v}$ ,  $\tilde{\mathbf{v}}$  is the skew-symmetric matrix associated to it.

<sup>4</sup>Gravity can be simply taken into account by setting  $\dot{\mathbf{v}}'_1 = -\mathbf{g}$ , where  $\mathbf{g}$  is the gravity acceleration in the world frame.

the spatial vector notation [20], consequently defining

$$\dot{\mathbf{V}}_i = \begin{bmatrix} \dot{\boldsymbol{\omega}}_i \\ \dot{\mathbf{v}}_i \end{bmatrix} \in \mathbb{R}^6, \quad (7)$$

Equations (5) and (6) can be represented in compact form, such as:

$$\dot{\mathbf{V}}_i - \mathbf{P}_{i-1} \dot{\mathbf{V}}_{i-1} = \mathbf{B}_{\theta,i-1} \ddot{\boldsymbol{\theta}}_i + \mathbf{B}_{q,i-1} \ddot{\mathbf{q}}_{i-1} + \dot{\mathbf{V}}_i', \quad (8)$$

where  $\mathbf{P}_i \in \mathbb{R}^{6 \times 6}$ ,  $\mathbf{B}_{\theta,i} \in \mathbb{R}^6$ ,  $\mathbf{B}_{q,i} \in \mathbb{R}^{6 \times M_i}$  are suitable matrices. Finally, defining  $\dot{\mathbf{V}} = \text{col}\{\dot{\mathbf{V}}_i\} \in \mathbb{R}^{6N}$ ,  $\dot{\mathbf{V}}' = \text{col}\{\dot{\mathbf{V}}_i'\} \in \mathbb{R}^{6N}$  eqs. (8) can be represented into a single global equation:

$$\mathcal{P}^T \dot{\mathbf{V}} = \mathcal{B}_\theta \ddot{\boldsymbol{\theta}} + \mathcal{B}_q \ddot{\mathbf{q}} + \dot{\mathbf{V}}', \quad (9)$$

where  $\mathcal{P} \in \mathbb{R}^{6N \times 6N}$ ,  $\mathcal{B}_\theta \in \mathbb{R}^{6N \times N}$ ,  $\mathcal{B}_q \in \mathbb{R}^{6N \times M}$ .

The dynamic equations of the manipulator can be computed starting from the well known Newton-Euler formulation of the motion equations for the  $i$ -th flexible link, which applies the principle of virtual works [10].

$$\begin{bmatrix} m_i \mathbf{U} & m_i \tilde{\mathbf{d}}_{C,i}^T & \tilde{\mathbf{C}}_{t,i}^T \\ m_i \tilde{\mathbf{d}}_{C,i} & \tilde{\mathbf{J}}_i & \tilde{\mathbf{C}}_{r,i}^T \\ \tilde{\mathbf{C}}_{t,i} & \tilde{\mathbf{C}}_{r,i} & \mathbf{M}_{e,i} \end{bmatrix} \begin{bmatrix} \dot{\mathbf{v}}_i \\ \dot{\boldsymbol{\omega}}_i \\ \dot{\mathbf{q}}_i \end{bmatrix} = \begin{bmatrix} \mathbf{0}_3 \\ \mathbf{0}_3 \\ -\mathbf{K}_{e,i} \mathbf{q}_i - \mathbf{D}_{e,i} \dot{\mathbf{q}}_i \end{bmatrix} + \begin{bmatrix} \mathbf{h}_{\omega,i}^r \\ \mathbf{h}_{\omega,i}^\theta \\ \mathbf{h}_{\omega,i}^f \end{bmatrix} + \begin{bmatrix} \mathbf{h}_{e,i}^r \\ \mathbf{h}_{e,i}^\theta \\ \mathbf{h}_{e,i}^f \end{bmatrix} \quad (10)$$

where matrix  $\mathbf{D}_{e,i}$ , modelling the dissipative properties of the material, can be defined as  $\mathbf{D}_{e,i} = \alpha_i \mathbf{M}_{e,i} + \beta_i \mathbf{K}_{e,i}$ , where  $\alpha_i$  and  $\beta_i$  are the so-called Rayleigh damping coefficients,  $\mathbf{h}_{\omega,i}^r \in \mathbb{R}^3$ ,  $\mathbf{h}_{\omega,i}^\theta \in \mathbb{R}^3$ ,  $\mathbf{h}_{\omega,i}^f \in \mathbb{R}^{M_i}$  are the vectors of gyroscopic and centripetal terms [25], and  $\mathbf{h}_{e,i}^r \in \mathbb{R}^3$ ,  $\mathbf{h}_{e,i}^\theta \in \mathbb{R}^3$ ,  $\mathbf{h}_{e,i}^f \in \mathbb{R}^{M_i}$  are the vectors of external forces, applied at the body connectors. The terms in the generalized mass matrix depend on the 9 inertia invariants listed in Table 1, which in turn depend on the shape functions and on the body mass distribution.

The vectors  $\mathbf{h}_{e,i}$  of external forces, relative to the world frame, can be computed by defining as  $\mathbf{f}_i$ ,  $\mathbf{n}_i$  the force and torque applied from link  $i - 1$

to link  $i$  at  $O_i$  as follows<sup>5</sup>:

$$\mathbf{h}_{e,i}^r = \bar{\mathbf{f}}_i - \bar{\mathbf{f}}_{i+1} , \quad (11)$$

$$\mathbf{h}_{e,i}^\theta = \bar{\mathbf{n}}_i - \bar{\mathbf{n}}_{i+1} - \tilde{\mathbf{u}}_i \bar{\mathbf{f}}_{i+1} , \quad (12)$$

$$\mathbf{h}_{e,i}^f = -\mathbf{S}_i^T \bar{\mathbf{f}}_{i+1} - \hat{\mathbf{S}}_i^T \bar{\mathbf{n}}_{i+1} , \quad (13)$$

Furthermore, by collecting torques and forces in a vector  $\mathbf{F}_i = [\mathbf{n}_i^T \mathbf{f}_i^T]^T \in \mathbb{R}^6$ , two equations can be obtained as follows:

$$\mathbf{I}_{vv,i} \dot{\mathbf{V}}_i + \mathbf{I}_{vq,i} \ddot{\mathbf{q}}_i - \mathbf{C}_{v,i} = \mathbf{F}_i - \mathbf{P}_i^T \mathbf{F}_{i+1} , \quad (14)$$

$$\mathbf{I}_{vq,i}^T \dot{\mathbf{V}}_i + \mathbf{M}_{e,i} \ddot{\mathbf{q}}_i = -\mathbf{K}_{e,i} \mathbf{q}_i - \mathbf{D}_{e,i} \dot{\mathbf{q}}_i + \mathbf{h}_{\omega,i}^f - \mathbf{B}_{q,i}^T \mathbf{F}_{i+1} , \quad (15)$$

where

$$\mathbf{I}_{vv,i} = \begin{bmatrix} \mathbf{A}_i \bar{\mathbf{J}}_i \mathbf{A}_i^T & m_i \mathbf{A}_i \tilde{\mathbf{d}}_{C,i}^T \mathbf{A}_i^T \\ m_i \mathbf{A}_i \tilde{\mathbf{d}}_{C,i}^T \mathbf{A}_i^T & m_i \mathbf{U} \end{bmatrix} \in \mathbb{R}^{6 \times 6} , \quad (16)$$

$$\mathbf{I}_{vq,i} = \begin{bmatrix} \mathbf{A}_i \bar{\mathbf{C}}_{r,i}^T \\ \mathbf{A}_i \bar{\mathbf{C}}_{t,i}^T \end{bmatrix} \in \mathbb{R}^{6 \times M_i} , \quad \mathbf{C}_{v,i} = \begin{bmatrix} \mathbf{A}_i \mathbf{h}_{\omega,i}^\theta \\ \mathbf{A}_i \mathbf{h}_{\omega,i}^r \end{bmatrix} \in \mathbb{R}^6 , \quad (17)$$

Defining  $\mathcal{F} = \text{col}\{\mathbf{F}_i\} \in \mathbb{R}^{6N}$ ,  $\mathcal{C}_v = \text{col}\{\mathbf{C}_{v,i}\} \in \mathbb{R}^{6N}$ ,  $\mathcal{C}_f = \text{col}\{\mathbf{h}_{\omega,i}^f\} \in \mathbb{R}^M$  the following global equations are obtained:

$$\mathcal{I}_{vv} \dot{\mathcal{V}} + \mathcal{I}_{vq} \ddot{\mathcal{q}} - \mathcal{C}_v = \mathcal{P} \mathcal{F} , \quad (18)$$

$$\mathcal{I}_{vq}^T \dot{\mathcal{V}} + \mathcal{M}_e \ddot{\mathcal{q}} + \mathcal{D}_e \dot{\mathcal{q}} + \mathcal{K}_e \mathcal{q} - \mathcal{C}_f = -\mathcal{B}_q^T \mathcal{F} , \quad (19)$$

with  $\mathcal{I}_{vv} \in \mathbb{R}^{6N \times 6N}$ ,  $\mathcal{I}_{vq} \in \mathbb{R}^{6N \times M}$ ,  $\mathcal{M}_e \in \mathbb{R}^{M \times M}$ ,  $\mathcal{K}_e \in \mathbb{R}^{M \times M}$ ,  $\mathcal{D}_e \in \mathbb{R}^{M \times M}$ .

Finally, by solving eq. (9) with respect to  $\dot{\mathcal{V}}$ , and eq. (18) with respect to  $\mathcal{F}$ , and substituting in eq. (19) one obtains eq. (2). Premultiplying eq. (18) by  $\mathcal{B}_\theta^T \mathcal{P}^{-1}$  and recalling that the joint input torque  $\tau_i$  is equal to the scalar product between the  $i$ -th joint rotation axis and torque  $\mathbf{n}_i$  so that

$$\boldsymbol{\tau} = \mathcal{B}_\theta^T \mathcal{F} , \quad (20)$$

---

<sup>5</sup>The bar above a vector means that the vector is expressed relative to the local FFR.

one obtains eq. (1) where<sup>6</sup>

$$\mathcal{M}_{\theta q}^T = \{ (\mathcal{I}_{vq}^T \mathcal{P}^{-T}) + [\mathcal{B}_q^T (\mathcal{P}^{-1} \mathcal{I}_{vv} \mathcal{P}^{-T})] \} \mathcal{B}_\theta, \quad (21)$$

$$\mathcal{M}_{qq} = \mathcal{M}_e + \mathcal{B}_q^T (\mathcal{P}^{-1} \mathcal{I}_{vv} \mathcal{P}^{-T}) \mathcal{B}_q + [(\mathcal{I}_{vq}^T \mathcal{P}^{-T}) \mathcal{B}_q] + [(\mathcal{I}_{vq}^T \mathcal{P}^{-T}) \mathcal{B}_q]^T,$$

$$\mathcal{C}_q = \{ (\mathcal{I}_{vq}^T \mathcal{P}^{-T}) + [\mathcal{B}_q^T (\mathcal{P}^{-1} \mathcal{I}_{vv} \mathcal{P}^{-T})] \} \dot{\mathbf{v}}' - \mathcal{B}_q^T (\mathcal{P}^{-1} \mathcal{C}_v) - \mathcal{C}_f, \quad (22)$$

$$\mathcal{M}_{\theta\theta} = [\mathcal{B}_\theta^T (\mathcal{P}^{-1} \mathcal{I}_{vv} \mathcal{P}^{-T})] \mathcal{B}_\theta, \quad (23)$$

$$\mathcal{C}_\theta = [\mathcal{B}_\theta^T (\mathcal{P}^{-1} \mathcal{I}_{vv} \mathcal{P}^{-T})] \dot{\mathbf{v}}' - \mathcal{B}_\theta^T (\mathcal{P}^{-1} \mathcal{C}_v). \quad (24)$$

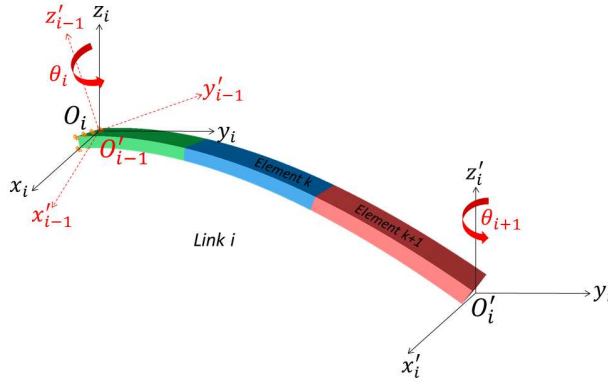


Figure 3: Substructuring a highly flexible bar into  $k + 1$  segments

In order to cope with a high flexibility, link  $i$  can be subdivided into more rigidly connected flexible elements or substructures, as shown in Fig. 3, each one described through a FFR approach introducing  $M_k$  modal coordinates. Define with  $N_e$  the total number of elements of the whole manipulator and with  $M = \sum_{k=1}^{N_e} M_k$  the total number of modal coordinates.

Let  $\theta_i = \theta_k^e, i = 1, \dots, N$  denote the “real” joint angle between element  $\bar{k} - 1$  and  $\bar{k}$ , consider a “dummy” joint angle  $\theta_k^e$  if a rigid connection exists between element  $k - 1$  and  $k$ , thus  $\theta_k^e = 0, \dot{\theta}_k^e = 0, \ddot{\theta}_k^e = 0$ . As a consequence, the model remains formally identical by removing the columns of matrix  $\mathcal{B}_\theta$  corresponding to the “dummy” joint angles and with matrices  $\mathcal{B}_q$  and  $\mathcal{B}_\theta$  having dimensions  $6N_e \times M$  and  $6N_e \times N$ , respectively.

<sup>6</sup>Matrix  $\mathcal{P}$  is invertible and can be directly computed without resorting to matrix inversion [25].

## 4. Case studies

This Section presents two examples of application of the closed form model, aiming to validate the model and the high flexibility extension. The first example concerns modelling of a three DOFs elastic manipulator. It aims at showing the accuracy, with respect to an experimental dataset, in reproducing the rigid and flexible dynamics of the robot. The second example, instead, is related to a simulation benchmark of a 3D highly flexible body [26], and aims at showing a comparison between the proposed modelling technique and the ANCF approach.

### 4.1. Modelling the flexible manipulator TUDOR

The closed-form model presented in Section 3 has been experimentally validated by means of the MERIt dataset [27], an online available set of experimental measurements collected using the TUDOR experimental platform, a three DOFs elastic manipulator designed by the Technische Universität Dortmund [28].

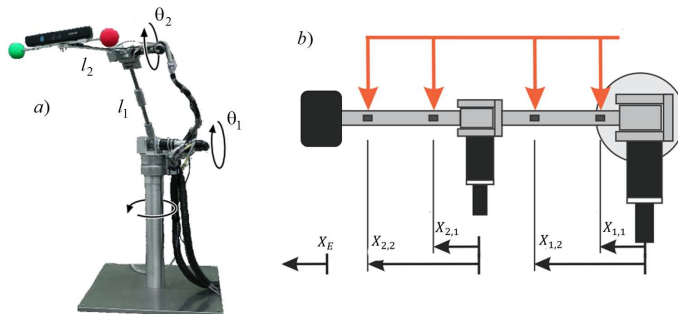


Figure 4: The TUDOR experimental platform

The base link of the robot is rigid and the first rotary joint moves the manipulator in the horizontal plane, while the second and third rotary joints move links  $l_1$  and  $l_2$  in a vertical plane, acting on joint angles  $\theta_1$  and  $\theta_2$  (Fig. 4a). Links  $l_1$  and  $l_2$  are made up by spring steel rods with rectangular cross-section, oriented in order to have great flexibility in the vertical plane. Link, joint and motor data are reported in [25].

Strain gauges are placed on each elastic rod, at  $X_{1,1} = 46$  mm and  $X_{1,2} = 260$  mm from the root of the first rod, and  $X_{2,1} = 45$  mm and  $X_{2,2} = 235$  mm from the root of the second rod (Fig. 4b).

Beam elements were used to model the two flexible links. An automatic procedure for node placement was adopted. This approach helps to retain the eigenmodes and the three corresponding lowest values of eigenfrequencies while discarding the  $2^{nd}$  out-of-plane eigenmode. Three strain gauge were used to obtain the simulated values from three nodes, each at a distance of 1.5 mm from a gauge. To this aim, the deflection of the three nodes has been calculated by means of the  $\mathbf{S}_i$  shape matrices then, a cubic function  $\phi(x) = Ax^3 + Bx^2 + Cx$  of the beam abscissa  $x$  has been computed by interpolation (the zero deflection of the FFR has been also considered). Finally, recalling that the strain  $\epsilon(x)$  is proportional to the second derivative of the deflection with respect to the beam abscissa, we have  $\epsilon(x) = 6Ax + 2B$ .

The experimental measurements provided by the MERIt dataset include joint angles and velocities, motor currents and strains measured along trajectories characterised by different payloads (0, 100, 200 and 400 g) and different pseudo-random joint position references. In order to reproduce the same trajectories with the simulator, two PID controllers have been manually tuned with the aim of correctly simulate the behaviour of the TUDOR manipulator in terms of joint positions.

Figures 5 and 6 show a comparison between the strain gauge measurements (black solid line) and the strain computed by the model (dashed grey line) on the second link at the same positions, in the case of a payload of 400 g. As it is apparent, there is a good accordance between the simulated model and the experimental data in terms of frequencies and overall behaviour, but the mean value of the computed strains is slightly higher with respect to the measurements. The phenomenon can be explained by a non-ideal placement of the strain gauges or the fact that the real material could differ from the theoretical characteristics. Moreover, table 2 shows the standard deviation between the simulated and measured signals with a payload of 0, 100, 200 and 400 g, covering all the configurations provided in MERIt and showing a nice robustness of the model with respect to different configurations.

#### *4.2. Modelling a highly flexible double pendulum*

High flexibility modelling has been validated by comparison of simulation results obtained with a MATLAB implementation of the closed-form model, with multibody simulations obtained with Modelica/Dymola and with MSC/Adams. The simulation benchmark has been taken from [26], where the ANCF is used to describe link compliance in the case of a flexible double pendulum.

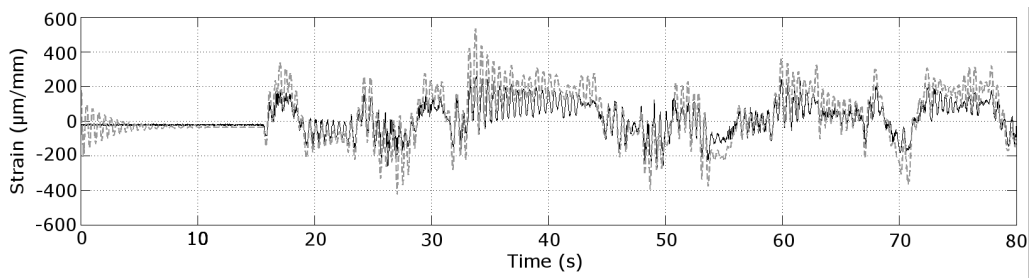


Figure 5: Comparison between strain gauge measurements (black solid line) and strain computed by MATLAB simulation (grey dashed line) at position  $X_{2,1}$

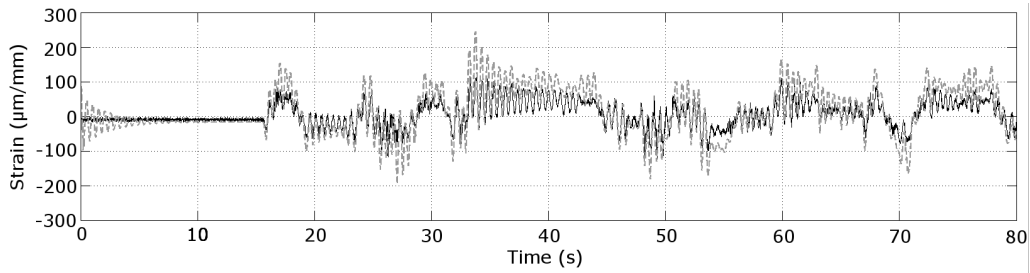


Figure 6: Comparison between strain gauge measurements (black solid line) and strain computed by MATLAB simulation (grey dashed line) at position  $X_{2,2}$ .

Table 2: Computed vs Measured strains: Standard deviation

Payload	Standard deviation ( $\mu m/mm$ )
0g	42.8
100g	39.7
200g	41.3
400g	36.9

The structure consists of two flexible bodies connected together and to the ground by revolute joints, initially in horizontal position and free to fall under the effect of gravity. The physical parameters have been chosen in order to allow large deformations on the second link. Substructuring has been implemented by subdividing the first link in 2 elements with length 0.1 m and the second link in 12 elements with length 0.075 m. FE preprocessing has been performed through the MSC Nastran/Patran suite: the elements of the first link have been modelled through 10 nodes connected by CBAR2 beam elements and 6 eigenmodes have been retained, while 12 elements have been considered for the second link, meshed with 20 nodes connected by CBAR2 elements, 6 eigenmodes were again retained.

A sequence of 3D snapshots of the simulation at intermediate time instants is shown in Fig. 7, while Figs. 8 and 9 show the absolute position of the tip of the second link, obtained with a MATLAB simulation (solid line), a Modelica/Dymola simulation (dashed line) and a MSC/Adams simulation (dotted line). As it is apparent, the results obtained from MATLAB and Modelica/Dymola simulations are undistinguishable, while the results provided by MSC/Adams show some small differences. In this respect, it must be pointed out that the Modelica model accounts for damping in exactly the same way as the closed-form model implemented in MATLAB does, while Adams adopts a different approach. In particular, the approach adopted in Modelica is based on the Rayleigh coefficients, applying a damping factor that is proportional to the frequency of the eigenvalue. On the other hand, Adams applies a damping constant factor to every considered eigenmode by default.

Figure 10 shows the transverse deflection of the tip of the second link. As before, results obtained from MATLAB and Modelica/Dymola are almost identical, while Adams simulation shows a very similar behaviour.

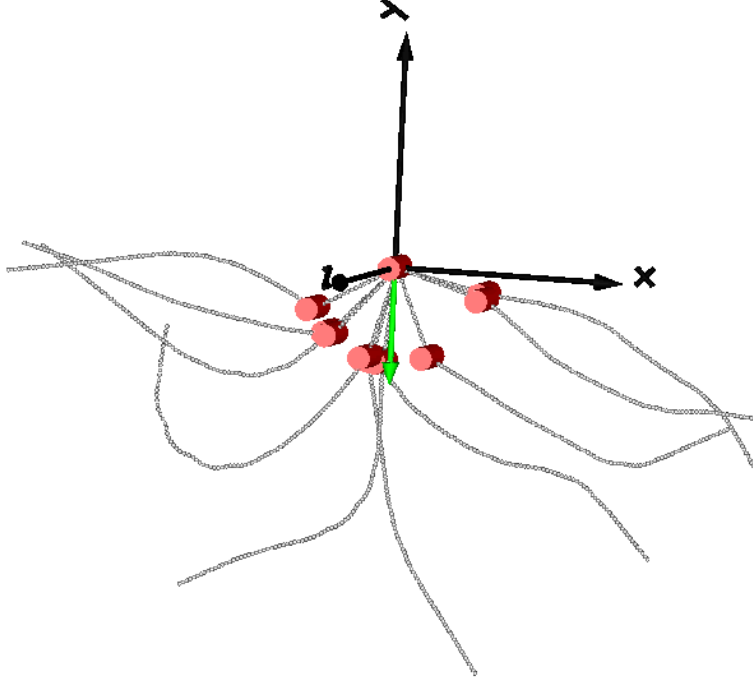


Figure 7: 3D representation of the double pendulum simulation

## 5. A control oriented model of a flexible system

This Section explains how the closed-form equations derived in Section 3 can be exploited to develop a control-oriented model based on the integral manifold approach, originally described in [29].

Defining with  $\mathcal{H}$  be the inverse of the symmetric, positive definite inertia matrix of the manipulator, the model described by eqs. (1) and (2) can be rewritten in singular perturbation form by assuming a suitable perturbation parameter  $\varepsilon$ , namely the inverse of the smallest stiffness matrix element:

$$\dot{\mathbf{x}}_1 = \mathbf{x}_2 \quad (25)$$

$$\dot{\mathbf{x}}_2 = -\mathcal{H}_{\theta\theta}\mathbf{C}_\theta - \mathcal{H}_{\theta q}\mathbf{C}_q + \mathcal{H}_{\theta\theta}\mathbf{u} - \mathcal{H}_{\theta q}\mathbf{z}_1 \quad (26)$$

$$\varepsilon\dot{\mathbf{z}}_1 = \mathbf{z}_2 \quad (27)$$

$$\varepsilon\bar{\mathcal{K}}_e^{-1}\dot{\mathbf{z}}_2 = -\mathcal{H}_{q\theta}\mathbf{C}_\theta - \mathcal{H}_{qq}\mathbf{C}_q + \mathcal{H}_{q\theta}\mathbf{u} - \mathcal{H}_{qq}\mathbf{z}_1 \quad (28)$$

where  $\mathbf{x}_1 = \boldsymbol{\theta}$ ,  $\mathbf{x}_2 = \dot{\boldsymbol{\theta}}$ ,  $\mathbf{z}_1 = \mathcal{K}_e\mathbf{q}$ ,  $\mathbf{z}_2 = \varepsilon\mathcal{K}_e\dot{\mathbf{q}}$ . Assume now that the control

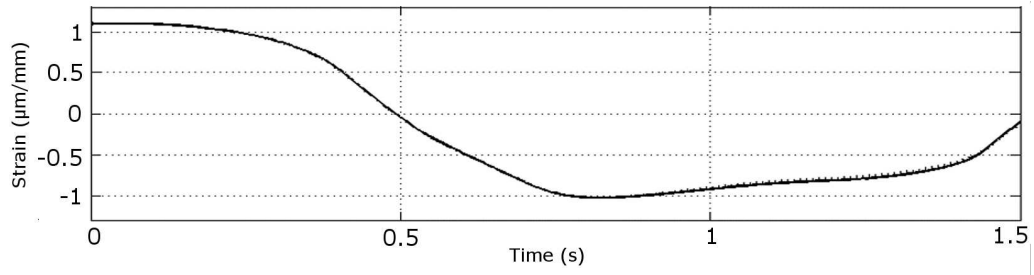


Figure 8: Absolute displacement of second link tip on X direction

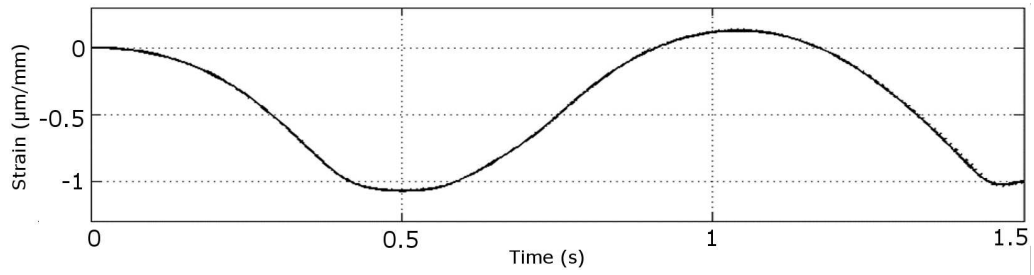


Figure 9: Absolute displacement of second link tip on Y direction

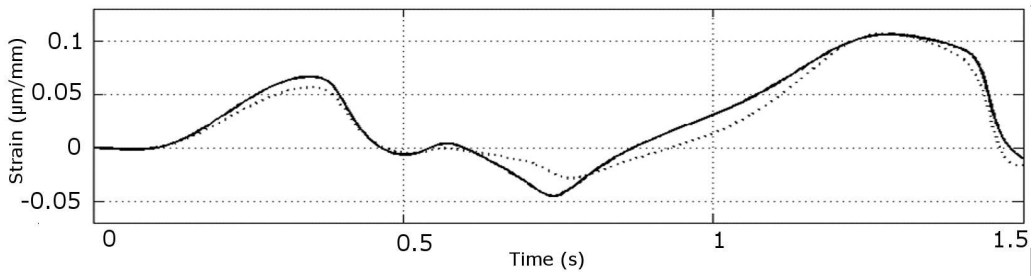


Figure 10: Transverse deflection of second link tip

input  $\mathbf{u}$  is decomposed into a slow input  $\bar{\mathbf{u}}$  and a fast input  $\mathbf{u}_f$ :

$$\mathbf{u} = \bar{\mathbf{u}} + \mathbf{u}_f \quad (29)$$

according to the integral manifold theory [30], the system lies on the manifold if the evolution of  $\mathbf{z}$  can be described by a surface  $\mathbf{h}$ , which, in turn, can be expressed as a function of the slow state  $\mathbf{x}$ , the slow input  $\bar{\mathbf{u}}$  and the perturbation parameter  $\varepsilon$ . If the manifold condition is satisfied, the on-manifold dynamics of the  $\mathbf{z}$  variables can be described as  $\mathbf{h}_{1,2}(\mathbf{x}_1, \mathbf{x}_2, \bar{\mathbf{u}}, \varepsilon)$ . The computation of the manifold condition  $\mathbf{h}$  involves the solution of a PDE, that is difficult to solve explicitly. An approximation of the solution, based on a series expansion with respect to  $\varepsilon$  can be considered, instead, recalling that the slow control input  $\bar{\mathbf{u}}$ , the inverse of the inertia matrix  $\mathcal{H}$ , and vectors  $\mathcal{C}_\theta$  and  $\mathcal{C}_q$  must be expanded as well. Thanks to the fact that vectors and matrices in the closed-form model (1,2) are defined by a product of factors [25, 31], the computation of their partial derivatives is feasible, even if lengthy. The distance from the manifold can be now defined, introducing a new set of coordinates  $\boldsymbol{\eta}$ , as follows:

$$\boldsymbol{\eta} = \mathbf{z} - \mathbf{h}(\mathbf{x}, t) \quad (30)$$

In order to cope with the off-manifold dynamics, a convenient time scale  $\tau = t/\varepsilon$  is introduced, and the system described in terms of the new coordinates is differentiated with respect to the  $\tau$  time scale:

$$\frac{d\boldsymbol{\eta}_1}{d\tau} = \boldsymbol{\eta}_2 \quad (31)$$

$$\frac{d\boldsymbol{\eta}_2}{d\tau} = - \left( \bar{\mathcal{H}}_{qq} + \varepsilon^2 \bar{\hat{\mathcal{H}}}_{qq} \right) \boldsymbol{\eta}_1 + \left( \bar{\mathcal{H}}_{q\theta} + \varepsilon^2 \bar{\hat{\mathcal{H}}}_{q\theta} \right) \mathbf{u}_f \quad (32)$$

Where  $\bar{\mathcal{H}}_{qq}$ ,  $\bar{\hat{\mathcal{H}}}_{qq}$ ,  $\bar{\mathcal{H}}_{q\theta}$  and  $\bar{\hat{\mathcal{H}}}_{q\theta}$  are the first and second order expansions of the submatrices of  $\mathcal{H}$ , respectively. According to the Tikhonov's theorem [30], if the equilibrium of the system on the manifold is asymptotically stable, the off-manifold set of coordinates  $\boldsymbol{\eta}$  is expected to quickly vanish in the  $t$  time scale.

On the other hand, the dynamics of the on-manifold system is given by:

$$\dot{\mathbf{x}}_1 = \mathbf{x}_2 \quad (33)$$

$$\begin{aligned} \dot{\mathbf{x}}_2 = & -\mathcal{H}_{\theta\theta} [\mathcal{C}_\theta - (\bar{\mathbf{u}}^0 + \bar{\mathbf{u}}^1 \varepsilon + \bar{\mathbf{u}}^2 \varepsilon^2)] - \mathcal{H}_{\theta q} (\mathcal{C}_q + \bar{\mathbf{z}}_1) \\ & - \varepsilon^2 \left[ \mathcal{H}_{\theta\theta} (\hat{\mathcal{C}}_\theta + \tilde{\mathcal{C}}_\theta^1) + \hat{\mathcal{H}}_{\theta\theta} (\mathcal{C}_\theta - \bar{\mathbf{u}}^0) \right] \\ & - \varepsilon^2 \left[ \mathcal{H}_{\theta q} (\hat{\mathcal{C}}_q + \tilde{\mathcal{C}}_q^1) + \hat{\mathcal{H}}_{\theta q} (\mathcal{C}_q + \mathbf{h}_1^0) \right] \end{aligned} \quad (34)$$

It must be pointed out that the off-manifold system is linear but time varying, and the varying parameter is  $\mathbf{x}_1$  which is expected to vary slowly with respect to the  $\tau$  time scale. Furthermore, the on-manifold dynamics only depend on the initial values of  $\boldsymbol{\eta}$  and on the control input  $\mathbf{u}_f$ , hence there is no influence of the slow dynamics on the fast system. The on-manifold system is instead highly non linear. This scenario naturally calls for two control schemes working in parallel, a slow control scheme for the gross motion and a fast control scheme aimed at vibration damping.

In order to validate the integral manifold model with respect to experimental data, the first case study has been considered. An integral manifold model of the TUDOR manipulator has been derived and implemented using Matlab/Simulink, and validated with respect to the MERIt [27] dataset.

As the theory of integral manifold lacks a rigorous procedure for the expansion of the control input in terms of  $\mathbf{u}_0$ ,  $\mathbf{u}_1$  and  $\mathbf{u}_2$ , in this preliminary stage the output of the PID regulators has been assigned entirely to  $\mathbf{u}_0$ . In this way both the on-manifold and the off-manifold dynamics have been excited, allowing for a comparison between MERIt experimental data (in grey dashed line) and simulation results (in black solid line).

Considering the validation of the on-manifold dynamics, the time evolution of the measured and computed strains is shown in Figure 11. It must be pointed out that the off-manifold system does not depend on the slow input, hence the  $\eta$  state variables are fixed to zero during the simulation. The flexible dynamics of the simulated model, which is considered to be on the manifold, is consequently a low frequency approximation of the original system.

The validation of the off-manifold system is much more involved. This system is linear and independent from the slow input and has been validated by comparing it, in the frequency domain, to the original complete model. The joint angles have been fixed to zero during the simulation, and a non-zero initial value has been assigned to the off-manifold state variables  $\boldsymbol{\eta}$ . The time evolution and frequency content of the tip transverse deflection have been compared to the corresponding quantity simulated with the complete model (described by Eqs. (1,2)). Figure 12 shows a comparison between the complete model (in dashed grey line) and the integral manifold model (in black solid line). Results demonstrate how the off-manifold system effectively reproduces the fast system dynamics. The initial perturbation of the fast system, and the corresponding perturbation of the  $\mathbf{q}$  variables in the complete model do not have a comparable physical meaning, hence the deflections

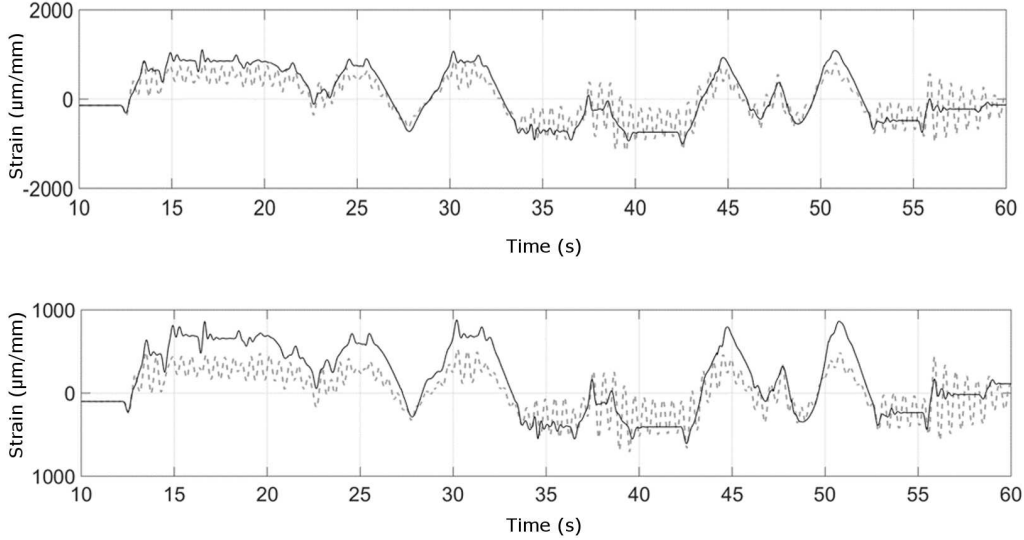


Figure 11: Strains on first link, comparison with original model

have been normalized in order to show the similar evolution in terms of vibration frequency, which can be further observed in the frequency domain plot. Considering that the integral manifold model is an approximation of the manipulator dynamics, developed for control purposes, results appear in good agreement with respect to experiments and complete model simulations.

## 6. Conclusion

In this paper, a control oriented model for 3D flexible manipulators with general link geometry, based on a closed-form model has been presented. The manipulator dynamics have been initially derived from the Newton-Euler equations of motion for the single flexible link, and a general procedure for the extraction of links' data has been outlined. The closed-form model of multiple link manipulators has been derived by means of the spatial vector notation and further improved by considering high flexibility of the links. A mathematical model for a two-link flexible manipulator has been developed, implemented, tested, and validated using an experimental platform (TUDOR) and an online experimental dataset (MERIt). The developed model performed well. Subsequently, the manipulator dynamics have been expressed in terms of the integral manifold approach, where the state-space

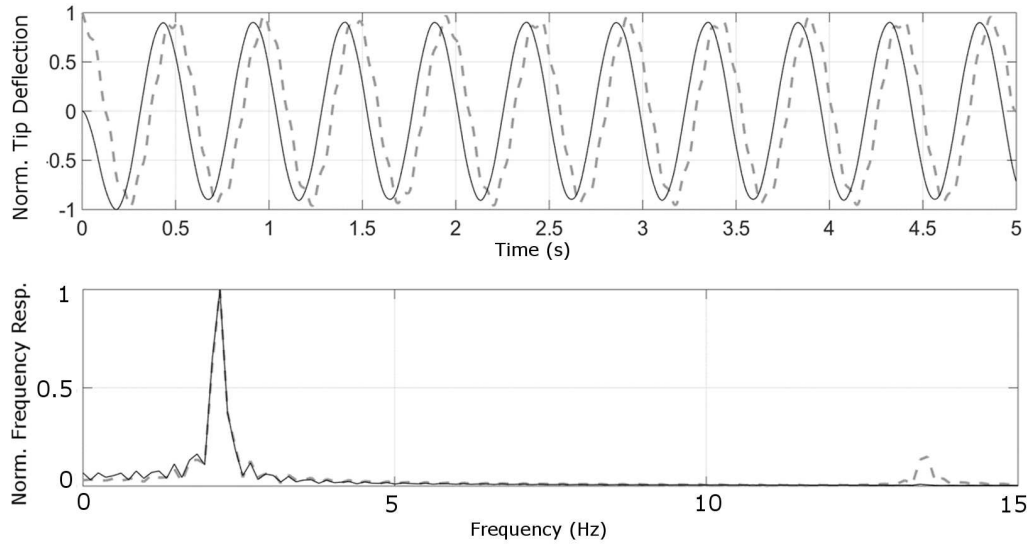


Figure 12: Perturbation of initial conditions on the fast system, comparison with original model

of the manipulator is split in two dynamical systems. It must be pointed out that the integral manifold approach can be considered as a refinement of the singular perturbation approach, developed in order to overcome the limitations of the singular perturbation approximation, and it must be recalled that the model described in this paper is nonetheless approximated.

Despite the approximation required to describe the manipulator dynamics in terms of the manifold, the model has been validated with respect to experimental results and with respect to a general formulation, where the complete dynamics is considered. The limitations of this work mainly concern the hypothesis of the integral manifold theory in which the frequency content of the on-manifold and off-manifold subsystems must be clearly separated, this restriction can be hard to fulfill with respect to the manipulator's design.

Further developments will include model based control, where the knowledge of fast dynamics will be exploited to develop an active vibration damping system.

## References

- [1] A. Albu-Schäffer, S. Haddadin, C. Ott, A. Stemmer, T. Wimböck, G. Hirzinger, The DLR lightweight robot: design and control concepts for robots in human environments, *Industrial Robot: An International Journal* 34 (5) (2007) 376–385.
- [2] E. Baumgartner, R. Bonitz, J. Melko, L. Shiraishi, P. Leger, The Mars Exploration Rover instrument positioning system, in: *IEEE Aerospace Conference*, 2005, pp. 1–19.
- [3] M. Kalyoncu, Mathematical modelling and dynamic response of a multi-straight-line path tracing flexible robot manipulator with rotating-prismatic joint, *Applied Mathematical Modelling* 32 (6) (2008) 1087–1098.
- [4] Z. Shi, E. H. Fung, Y. Li, Dynamic modelling of a rigid-flexible manipulator for constrained motion task control, *Applied Mathematical Modelling* 23 (7) (1999) 509–525.
- [5] EU FP7 Project HEPHESTOS, <http://www.hephestosproject.eu>.
- [6] G. G. Rigatos, Model-based and model-free control of flexible-link robots: A comparison between representative methods, *Applied Mathematical Modelling* 33 (10) (2009) 3906–3925.
- [7] W. J. Book, Recursive Lagrangian dynamics of flexible manipulator arms, *The international Journal of Robotics Research* 3 (3) (1984) 87–101.
- [8] A. De Luca, B. Siciliano, Closed-form dynamic model of planar multilink lightweight robots, *Systems, Man and Cybernetics, IEEE Transactions on* 21 (4) (1991) 826–839.
- [9] M. Rognant, E. Courteille, P. Maurine, A systematic procedure for the elastodynamic modeling and identification of robot manipulators, *Robotics, IEEE Transactions on* 26 (6) (2010) 1085–1093.
- [10] A. A. Shabana, *Dynamics of Multibody Systems*, Cambridge University Press, New York, 1998.

- [11] Dassault Systemès, Dassault Systèmes Simulia Corp. Abaqus Analysis Users Manual, Version 6.9. (2009).
- [12] MSC Software, MSC/NASTRAN Reference Manual, Version 68 – Lahey, Miller, et al. (1994).
- [13] W. Hurty, Dynamic analysis of structural systems using component modes, *AIAA Journal* 3 (4).
- [14] R. R. Craig, M. C. C. Bampton, Coupling of substructures for dynamic analyses, *AIAA Journal* 6 (7) (1968) 1313–1319.
- [15] C. C. Paige, B. N. Parlett, H. A. van der Vorst, Approximate solutions and eigenvalue bounds from Krylov subspaces, *Numerical Linear Algebra with Applications* 2 (2) (1995) 115—133.
- [16] H. V. Ly, H. T. Tran, Modeling and control of physical processes using proper orthogonal decomposition, *Mathematical and Computer Modelling* 33 (13) (2001) 223–236.
- [17] C. Nowakowski, J. Fehr, M. Fischer, P. Eberhard, Model order reduction in elastic multibody systems using the floating frame of reference formulation, in: *7<sup>th</sup> Vienna International Conference on Mathematical Modelling – MATHMOD 2012*, Vienna, Austria, 2012.
- [18] J. Escalona, H. Hussien, A. Shabana, Application of the absolute nodal coordinate formulation to multibody system dynamics, *Journal of Sound and Vibration* 214 (5) (1998) 833–851.
- [19] A. Shabana, Substructure synthesis methods for dynamic analysis of multibody systems, *Computers and Structures* 20 (4) (1985) 737 – 744.
- [20] A. Fijany, R. Featherstone, A new factorization of the mass matrix for optimal serial and parallel calculation of multibody dynamics, *Multibody System Dynamics* 29 (2013) 169–187.
- [21] G. Ferretti, B. Scaglioni, A. Rossi, Multibody model of a motorbike with a flexible swingarm, in: *Proceedings of the 10th international Modelica Conference*, Lund, March 10-12 2014, 2014.

- [22] M. Spong, K. Khorasani, P. Kokotovic, An integral manifold approach to the feedback control of flexible joint robots, *IEEE Journal of Robotics and Automation* 3 (4) (1987) 291–300.
- [23] L. Bascetta, P. Rocco, Two-time scale visual servoing of eye-in-hand flexible manipulators, *IEEE Transactions on Robotics* 22 (4) (2006) 818–830.
- [24] F. Schiavo, L. Viganò, G. Ferretti, Object-oriented modelling of flexible beams, *Multibody System Dynamics* 15 (3) (2006) 263–286.
- [25] L. Bascetta, G. Ferretti, B. Scaglioni, Closed-form Newton–Euler dynamic model of flexible manipulators, *Robotica* (in press).
- [26] R. Yakoub, A. Shabana, Use of Cholesky coordinates and the absolute nodal coordinate formulation in the computer simulation of flexible multibody systems, *Nonlinear Dynamics* 20 (3) (1999) 267–282.
- [27] A Multi-Elastic-Link Robot Identification Dataset, Institute of Control Theory and Systems Engineering, RST, TU Dortmund, Germany (2014).  
URL <http://tinyurl.com/TUDOR-MERIt>
- [28] R. F. R. Malzahn, J., T. Bertram, Dynamics identification of a damped multi elastic link robot arm under gravity, in: *IEEE International Conference on Robotics and Automation*, Honkong, China, 2014.
- [29] B. Siciliano, W. Book, G. Maria, An integral manifold approach to control of a one link flexible arm, in: *Proceedings of the IEEE Conference on Decision and Control*, 1986, pp. 1131–1134.
- [30] V. Sobolev, Integral manifolds and decomposition of singularly perturbed systems, *Systems and Control Letters* 5 (3) (1984) 169–179.
- [31] M. Baur, Control oriented model for 3D flexible manipulators, Master’s thesis, Politecnico di Milano (2015).